Int. J. Heat Mass Transfer. Vol. 15, pp. 1905–1932. Pergamon Press 1972. Printed in Great Britain

THE CALCULATION OF TURBULENT BOUNDARY LAYERS WITH FOREIGN GAS INJECTION†

R. B. LANDIS‡ and A. F. MILLS

Energy and Kinetics Dept., University of California, Los Angeles, California, U.S.A.

(*Received* 16 *September* 1971 *and in revised form* 26 *November* 1971)

Abstract—Numerical solutions have been obtained for flat plate compressible turbulent boundary layers of air with foreign gas injection, on the hypothesis that the momentum equation is coupled to the species and energy equations only through spatial variations of the mean density and viscosity. The finite difference calculation procedure incorporates the "ω^2" transformation with central differencing. The injected species include H_2, He, CH_4, H_2O, CO, Air, CO_2, Freon 12, Xe and CCl_4; temperature ratios T_s/T_e range from 0·2 to 2·0 while the Mach numbers range from 0 to 6. Thermodynamic properties are estimated allowing for variable specific heats; for the transport properties, kinetic theory with the Lennard-Jones potential is used. Thermal diffusion and diffusional conduction are ignored. Eddy viscosity models for the inner region were evaluated by comparison with experimental data for blown constant property flows, and a "best" model selected for the parametric calculations. The turbulent Schmidt and Prandtl numbers were taken as constants, respectively 0·8 and 0·9. The results show the important role played by density variations across the boundary layer; the mass and heat transfer Stanton numbers for the heaviest injectants actually increase with injection, and the light injectants are found to be more effective in reducing skin friction and heat transfer than experimental data indicate. Agreement with experiment for low speed flows is shown to be generally satisfactory; also, the predicted influence of Mach number on skin friction is found to be consistent with experiment.

NOMENCLATURE

A, Van Driest constant, equation (17);
B_f, skin friction blowing parameter $\equiv 2F/C_f^*$;
B_h, heat transfer blowing parameter $\equiv F/St_h^*$;
B_m, mass transfer blowing parameter $\equiv F/St_m^*$;
C_{eff}, $\rho\mu_{\text{eff}}/\rho_e\mu_e$;
C_f, skin friction coefficient $\equiv 2\tau_s/\rho_e u_e^2$;
C_p, specific heat;
DF, damping factor; equation (16);
$\mathscr{D}$, binary diffusion coefficient;
F, $\equiv \dot{m}/\rho_e u_e$;
j, species diffusion flux;
K, von Kármán constant, equation (15);
k, thermal conductivity;
l, Prandtl's mixing length;
M, Mach number, and molecular weight;
m, mass fraction;
$\dot{m}$, mass transfer rate;
Pr, Prandtl number $\equiv C_p\mu/k$;
q, conductive heat flux;
Re_x, Reynolds number based on length from leading edge;
Re_θ, Reynolds number based on momentum thickness;
$\mathscr{R}$, universal gas constant;
Sc, Schmidt number $\equiv \mu/\rho\mathscr{D}_{12}$;
St_h, heat transfer Stanton number, $q_s/\rho_e u_e(h_e - h_{es})$;
St_m, mass transfer Stanton number, $j_{1.s}/\rho_e u_e(m_{1.s} - m_{1.e})$;
T, temperature;
u, v, velocity components;
v^+, dimensionless normal velocity $\equiv v/\sqrt{(\tau_s/\rho)}$;
x, y, streamwise and normal coordinates, respectively;

† Computer time for the numerical calculations was supplied by the Campus Computing Network of the University of California, Los Angeles.

‡ Presently at San Fernando Valley State College, School of Engineering, Northridge, California.

y^+, dimensionless normal coordinate $\equiv y\sqrt{(\tau_s/\rho)}/\nu$;
δ, boundary layer thickness;
ε, maximum attractive energy between two molecules;
ε_M, eddy diffusivity of momentum;
θ, momentum thickness;
κ, Boltzman constant;
μ, dynamic viscosity;
ν, kinematic viscosity;
σ, collision diameter;
σ_{eff}, defined by equation (9);
ρ, density;
τ, shear stress;
ϕ, generalized dependent variable, equation (9);
ψ, stream function;
ω, defined by $\omega^2 \equiv (\psi - \psi_I)/(\psi_E - \psi_I)$.

Subscripts

a, value of y defined by equation (20);
E, outer edge of boundary layer;
e, free stream;
es, fluid of free stream composition at the surface temperature;
eff, effective $\equiv$ molecular + turbulent;
I, inner edge of boundary layer;
i, chemical species i, and i'th node across boundary layer;
s, surface;
t, turbulent;
1, 2, injected and free stream species, respectively.

Superscripts

*, zero injection value;
′, explicit evaluation, i.e. at the upstream station.

INTRODUCTION

THE CALCULATION of turbulent boundary layers with foreign gas injection finds many applications in engineering practice. Specific problems of current interest include transpiration, ablative and film cooling; more generally the problem area includes a great variety of vaporization and combustion processes. Of primary concern is the reduction, due to mass injection, of the wall shear stress, the mass transfer conductance, and the heat transfer rate. The problem parameters are many: Reynolds number, Mach number, temperature ratio, temperature level, injectant distribution and the injectant gas species. Even the turbulence model, and its associated empirical constants, must be viewed as parameters to be varied.

Jeromin [1] has recently published a comprehensive evaluation of the status (1966) of research into turbulent boundary layers with gas injection. An examination of his comparisons between theoretical predictions and experimental data for foreign gas injection suggests that one can have confidence in neither theory nor experiment for engineering use. The most notable predictive theories are those developed by Spalding, Auslander and Sundaram in 1964 [2], Ness in 1961 [3], and Rubesin and Pappas in 1958 [4]. The lack of any significant further theoretical development has been due to (i) the lack of an exact solution procedure for the governing equations, (ii) the large amount of empirical input required owing to poor understanding of turbulent transport mechanisms, and (iii) the paucity of reliable experimental data which would assist validation.

The art of predicting general turbulent boundary layers has advanced rapidly with the development of efficient finite difference procedures for the solution of the time averaged turbulent boundary layer equations; the most influential contribution was undoubtedly the book and computer program published by Patankar and Spalding in 1967 [5]. Thus there are now available the required exact solution procedures, and the first of the above mentioned obstacles to progress on the foreign gas injection problem can be removed. Of particular significance is that the finite difference approach allows the variable thermophysical properties characteristic of binary mixtures to be included, for it is easy to calculate exactly the mixture properties at each node point. Also, it becomes

feasible to systematically evaluate the consequences of physical hypotheses and empirical constants relating to the turbulent transport model; in this manner the critical features of a particular model can be readily identified.

The general objective of our study was to develop a calculation method suitable for both research and engineering design purposes. The path we followed is outlined below.

1. The overall complexity of calculating binary turbulent boundary layers made it necessary to expend considerable effort to explore and improve existing numerical procedures, until predetermined accuracy criteria could be reliably met within an acceptable computing cost. Our numerical procedure and final computer program have a number of innovations of utility for foreign gas injection, as well as for the calculation of turbulent boundary layers in general. Particularly noteworthy is the use of the "ω^2" transformation [6, 7] with central difference coefficients in the finite difference analogs.

2. Various eddy diffusivity models which account for mass transfer in constant property boundary layers were evaluated by making comparisons with experimental data for air into air injection. The experimental results most heavily relied upon were the skin friction data of Simpson *et al.* [8] and McQuaid [9], and the heat transfer data of Moffat and Kays [10]. A "best" model was selected for the purposes of making parametric studies.

3. Compressible turbulent boundary layers with foreign gas injection were calculated on the hypothesis that the momentum equation is coupled to the species and energy equations only through spatial variations of the mean density and viscosity. The significant trends exhibited by the results were explained in terms of features of the eddy diffusivity model and by comparison with exact solutions of binary laminar boundary layers. The critical role played by density variation was validated by performing calculations with synthetic injectants, and through comparisons with established results for the effect of wall cooling on unblown compressible boundary layers.

4. Comparisons were made with experimental data for low speed flows, and adequate agreement was shown. For high speed flows the effect of Mach number on skin friction was examined in detail; it was found necessary to carefully account for the effect of wall to free stream ratio in order to resolve apparent anomalies in the experimental data.

In our view the contribution of the present study is that we have taken the hypotheses of established validity for constant property and compressible boundary layers, and demonstrated their implications for foreign gas injection. Our results presented here are of use for simple engineering estimates. Furthermore, many engineering problems involve complicating factors such as nonuniform injection distribution or a streamwise pressure gradient. These problems require direct use of a calculation procedure similar to the present one; our results show the gross features to be expected when such flows are calculated.

ANALYSIS AND NUMERICAL PROCEDURE

Analysis

The conservation equations for steady turbulent boundary layer flow along a flat plate of an inert binary gas mixture may be written

mass:

$$\frac{\partial}{\partial x}(\rho u) + \frac{\partial}{\partial y}(\rho v) = 0 \tag{1}$$

momentum:

$$\rho u \frac{\partial u}{\partial x} + \rho v \frac{\partial u}{\partial y} = \frac{\partial}{\partial y}\left(\mu_{\text{eff}} \frac{\partial u}{\partial y}\right) \tag{2}$$

species:

$$\rho u \frac{\partial m_1}{\partial x} + \rho v \frac{\partial m_1}{\partial y} = \frac{\partial}{\partial y}\left(\frac{\mu_{\text{eff}}}{Sc_{\text{eff}}} \frac{\partial m_1}{\partial y}\right) \tag{3}$$

energy:

$$\rho u \frac{\partial T}{\partial x} + \rho v \frac{\partial T}{\partial y} = \frac{\partial}{\partial y}\left(\frac{\mu_{\text{eff}}}{Pr_{\text{eff}}} \frac{\partial T}{\partial y}\right)$$

$$+\frac{1}{C_p}\left[\frac{\mu_{\text{eff}}}{Pr_{\text{eff}}}\frac{dC_p}{dT}\left(\frac{\partial T}{\partial y}\right)^2+\frac{\mu_{\text{eff}}}{Sc_{\text{eff}}}(C_{p1}-C_{p2})\frac{\partial m_1}{\partial y}\frac{\partial T}{\partial y}+\mu_{\text{eff}}\left(\frac{\partial u}{\partial y}\right)^2\right] \quad (4)$$

where we have ignored thermal diffusion and diffusional conduction. The viscous dissipation term in equation (4) assumes that convection and diffusion of turbulent kinetic energy are negligible, i.e. the dissipation is equal to the local production. The effective transport coefficients are defined by the relations

$$\mu_{\text{eff}} = \mu + \rho\varepsilon_M \quad (5)$$

$$\frac{\mu_{\text{eff}}}{Sc_{\text{eff}}} = \frac{\mu}{Sc} + \frac{\rho\varepsilon_M}{Sc_t}; \quad \frac{\mu_{\text{eff}}}{Pr_{\text{eff}}} = \frac{\mu}{Pr} + \frac{\rho\varepsilon_M}{Pr_t}. \quad (6)$$

The boundary conditions imposed on the set of equations are

$$y = 0; u = 0; \rho v|_s = \dot{m};$$

$$-\rho\mathscr{D}_{12}\frac{\partial m_1}{\partial y}\bigg|_s = \dot{m}(1 - m_{1,s}); T = T_s \quad (7)$$

$$y \to \infty; u \to u_e; m_1 \to 0; T \to T_e. \quad (8)$$

Initial conditions will be discussed later, in connection with the numerical procedure.

The finite difference analog to the partial differential equations evolved from a procedure originally proposed by Patankar and Spalding [5]. For this purpose it is required to effect a transformation of the independent variables, x, y to x, ω. We use an improved transformation which was developed in [6] and [7], wherein ω is defined by the relation

$$\omega^2 = \int_0^y \rho u\,dy \Big/ \int_0^{y_e} \rho u\,dy = (\psi - \psi_I)/(\psi_E - \psi_I)$$

$$= (\psi - \psi_I)/\Delta\psi.$$

Subscripts I and E denote, respectively, the inner and outer edges of the boundary layer. Equations (2)–(4) transform into the general form

$$2\omega\frac{\partial\phi}{\partial x} + (A + B\omega^2)\frac{\partial\phi}{\partial\omega} = \frac{\partial}{\partial\omega}\left(C\frac{\partial\phi}{\partial\omega}\right) + S \quad (9)$$

where

$$A = -(d\psi_I/dx)/\Delta\psi;$$

$$B = -(d\psi_E/dx - d\psi_I/dx)/\Delta\psi,$$

and

$$C = (\mu_{\text{eff}}/\sigma_{\text{eff}})\,\rho u/2\omega\Delta\psi^2.$$

The source term S is zero for the momentum and species equations, and for the energy equation is given by

$$S = \frac{1}{C_p}\frac{\rho u}{2\omega\Delta\psi^2}\left[\frac{\mu_{\text{eff}}}{Pr_{\text{eff}}}\frac{dC_p}{dT}\left(\frac{\partial T}{\partial\omega}\right)^2 + \frac{\mu_{\text{eff}}}{Sc_{\text{eff}}}(C_{p1} - C_{p2})\frac{\partial m_1}{\partial\omega}\frac{\partial T}{\partial\omega} + \mu_{\text{eff}}\left(\frac{\partial u}{\partial\omega}\right)^2\right]. \quad (10)$$

Numerical procedure

The general conservation equation, equation (9), was approximated in finite difference form as

$$2\omega_i\frac{\phi_i - \phi_i'}{\Delta x} + \frac{(A' + B'\omega_i^2)}{\nabla_i + \nabla_{i+1}}\left[\frac{\nabla_i}{\nabla_{i+1}}(\phi_{i+1} - \phi_i) + \frac{\nabla_{i+1}}{\nabla_i}(\phi_i - \phi_{i-1})\right] = \frac{2}{\nabla_i + \nabla_{i+1}}\left[\left(\frac{C_{i+1}' + C_i'}{2}\right)\left(\frac{\phi_{i+1} - \phi_i}{\nabla_{i+1}}\right) - \left(\frac{C_i' + C_{i-1}'}{2}\right)\left(\frac{\phi_i - \phi_{i-1}}{\nabla_i}\right)\right] + S_i' \quad (11)$$

where primes denote explicit evaluation, and $\nabla_i = \omega_i - \omega_{i-1}$, $\nabla_{i+1} = \omega_{i+1} - \omega_i$. Equation (11) was cast in the form

$$\phi_i = A_i\phi_{i+1} + B_i\phi_{i-1} + C_i; \quad i = 2, 3, \ldots, N \quad (12)$$

which is solved for the ϕ_i's using an efficient tridiagonal matrix elimination algorithm. Treatment of Dirichlet type boundary conditions is straightforward since the dependent variable is specified at nodes $1(\omega = 0)$ and $N + 1$ $(\omega = 1)$. For the mixed boundary condition at the wall

for the species equation, the gradient $\partial\phi/\partial\omega$ was expressed in terms of ϕ_1, ϕ_2 and ϕ_3 using a second order forward difference interpolating polynomial. The boundary condition then assumes the form

$$\phi_1 = \alpha\phi_2 + \beta\phi_3 + \gamma \tag{13}$$

which is used to eliminate the unknown ϕ_1, from the set, equation (12), when $i = 2$. Wall gradients of the dependent variables were extracted directly in the ω-plane using the relation

$$\left.\frac{\partial\phi}{\partial y}\right|_s = \frac{\rho}{2\Delta\psi}\left.\frac{\partial u}{\partial\omega}\right|_s \left.\frac{\partial\phi}{\partial\omega}\right|_s \tag{14}$$

with second order polynomial fits of u and ϕ in terms of values at nodes 1, 2 and 3. To verify computational accuracy, the skin friction was also computed using the momentum integral equation. Other features of the finite difference procedure closely follow Patankar and Spalding [5]; further details may be found in [11]. Initial conditions, in the form of starting profiles for the dependent variables, are obtained from a numerical solution of the Couette flow approximation to the governing equations. The width of the Couette flow layer was adjusted until the momentum thickness matched that of a corresponding blown boundary layer.

Not less than 100 node points were distributed across the boundary layer, with a higher density near the wall. Although smaller forward steps were used for many calculations, a step-size of $\Delta x = \delta$ was found to yield sufficient accuracy, with a significant decrease in computer time. All computations were made on an IBM 360/91 computer with a FORTRAN-H compiler; 8·7 s of computer time were required to march from $Re_x = 2 \times 10^5$ to 10^7 (about 150 marching steps) with 100 cross-stream nodes.

Thermophysical properties

Species specific heats were taken from [12], except for H_2 [13] and Freon 12 [14]. Mixture values of the thermodynamic properties were calculated assuming ideal gas laws. Species transport properties were calculated according to the kinetic theory of gases with the Lennard–Jones interaction potential; parameters were taken from [12], except for Freon 12 [15]. Mixture transport properties were estimated using Wilke's mixing rule, as described in [16]. Table 1 lists representative property values.

TURBULENT TRANSPORT MODELS

In deriving the conservation equations, the second order correlations of fluctuating components were eliminated by introducing the eddy diffusivities of momentum, species and heat. The eddy diffusivities of species and heat were further eliminated in favor of the turbulent Schmidt and Prandtl numbers. Our purpose here is to discuss the selection of models for ε_M, Sc_t and Pr_t appropriate to flows with mass injection. In modeling ε_M it is customary to divide the flow into two regions; an inner region where turbulent transport is dominated by the presence of the wall, and an outer wake-like region. Reliable description of the turbulent transport in the inner region is more important since most of the change in the dependent variables takes place there.

Models for ε_M

We are concerned only with models which are continuous across the inner region; the earlier two-layer models [3, 4] have a physically unrealistic sharp discontinuity in ε_M at the edge of the laminar sub-layer, and also have been rendered obsolete by the use of finite difference solution procedures. Of the available models, the most significant are those of Patankar–Spalding [5], Cebeci [17], Kinney–Sparrow [18] and Powell–Strong [19]. For the unblown case each of these models becomes essentially Prandtl's mixing length model modified by van Driest's damping factor near the wall,

$$\varepsilon_M = (Ky)^2\,[1 - \exp(-y^+/26)]^2\left|\frac{du}{dy}\right| \tag{15}$$

Table 1. Thermodynamic and transport properties of the injected gases at 295 K

Species	M	$\frac{M}{M_{air}}$	$\frac{C_p}{C_{p,air}}$	$\frac{\mu}{\mu_{air}}$	$\frac{k}{k_{air}}$	Sc_v
H_2	2·016	0·0696	14·29	0·481	6·88	0·206
He	4·003	0·1382	5·18	1·10	5·90	0·219
CH_4	16·04	0·5537	2·17	0·606	1·30	0·705
H_2O	18·02	0·6220	1·87	0·592	1·10	0·726
CO	28·01	0·9669	1·03	0·959	0·989	0·763
Air	28·97	1·000	1·00	1·00	1·00	0·760
CO_2	44·01	1·519	0·832	0·821	0·67	1·00
Freon-12	120·9	4·174	0·592	0·676	0·379	1·65
Xe	131·3	4·532	0·158	1·250	0·204	1·24
CCl_4	153·8	5·310	0·538	0·531	0·269	2·06

with $y^+ \equiv y\sqrt{(\tau_s/\rho)}/\nu$. The effects of blowing are accounted for by modifications of the exponent in the damping factor, which for all the models has the general form

$$DF = 1 - \exp(-y/A). \tag{16}$$

The exponent y/A can be non-dimensionalized with the local shear stress as

$$\frac{y}{A} = \frac{y\sqrt{(\tau/\rho)}/\nu}{A\sqrt{(\tau/\rho)}/\nu} = \frac{y\sqrt{(\tau_s/\rho)}/\nu}{A\sqrt{(\tau/\rho)}/\nu} \times \sqrt{\left(\frac{\tau}{\tau_s}\right)} = \frac{y^+}{A\sqrt{(\tau/\rho)}/\nu}\sqrt{\left(\frac{\tau}{\tau_s}\right)}. \tag{17}$$

Reduction to the van Driest expression for the unblown case, $y/A = y^+/26$, can be ensured by setting $A\sqrt{(\tau/\rho)}/\nu = 26$, yielding

$$DF = 1 - \exp\left(-\frac{y^+}{26}\sqrt{\frac{\tau}{\tau_s}}\right), \tag{18}$$

which is the expression recommended by Patankar and Spalding. The Cebeci model differs from the Patankar–Spalding model only in that the exponent y/A is non-dimensionalized with the shear stress at the edge of the laminar sub-layer, taken to be at $y^+ = 11{\cdot}8$. This model is usually presented in a form derived from a Couette flow approximation for τ/τ_s in the near wall region. The momentum equation is written

$$\frac{d\tau}{dy} = \frac{v_s\tau}{\nu},$$

integrating to y_a with $\tau = \tau_s$ at $y = 0$ gives

$$\frac{\tau_a}{\tau_s} = \exp\left(\frac{v_s y_a}{\nu}\right) = \exp(y_a^+ v_s^+). \tag{19}$$

Substituting in equation (18) gives the damping factor as

$$DF = 1 - \exp\left(-\frac{y^+}{26}\sqrt{\exp(y_a^+ v_s^+)}\right), \tag{20}$$

and with $y_a^+ = 11{\cdot}8$

$$DF = 1 - \exp\left(-\frac{y^+}{26}\sqrt{\exp(11{\cdot}8\, v_s^+)}\right). \tag{21}$$

The Kinney–Sparrow and Powell–Strong models are extensions of the van Driest damping factor obtained by re-solving the Stoke's flow problem including mass transfer through the plate. In this formulation, the damping of the velocity field produced by an oscillating plate, through which mass is flowing, is determined by solving the time-dependent momentum equation.

$$\frac{\partial u}{\partial t} + v_s\frac{\partial u}{\partial y} = \nu\frac{\partial^2 u}{\partial y^2}$$

subject to the boundary condition $u = u_0\cos\omega t$ at the plate surface. Transposing the solution of this problem to the case of a stationary plate with an oscillating fluid, following the argument of van Driest, yields the Kinney–Sparrow damping factor. The Powell–Strong model in-

corporates additional empirical adjustment based on experimental data.

Turning now to the wake region, the mixing length expression proposed by Simpson [21]

$$l = \frac{K}{4}\delta\left[1 - \exp\left(-\frac{4y}{\delta}\right)\right] \tag{22}$$

is probably the most appropriate for blown flat plate boundary layers. This expression is a little different to that of Escudier [22], which was recommended by Patankar and Spalding [5]; as shown by Simpson it provides a better fit to both the unblown experimental data of Klebanoff [23], and the blown data of Simpson [8]. The dividing line between the inner and outer regions is determined by requiring that ε_M be continuous.

Since all models reduce to the same expression for the unblown case, comparison with unblown experimental data was utilized to select von Kármán's constant K. The wall shear stress was calculated for incompressible flow with two often used values of K: 0·4 and 0·435, and also following Simpson [21], i.e. $K = 0{\cdot}4$ for $Re_\theta \geqslant 6000$ and $K = 0{\cdot}4\ (Re_\theta/6000)^{-\frac{1}{8}}$ for $Re_\theta < 6000$. The comparison with the unblown

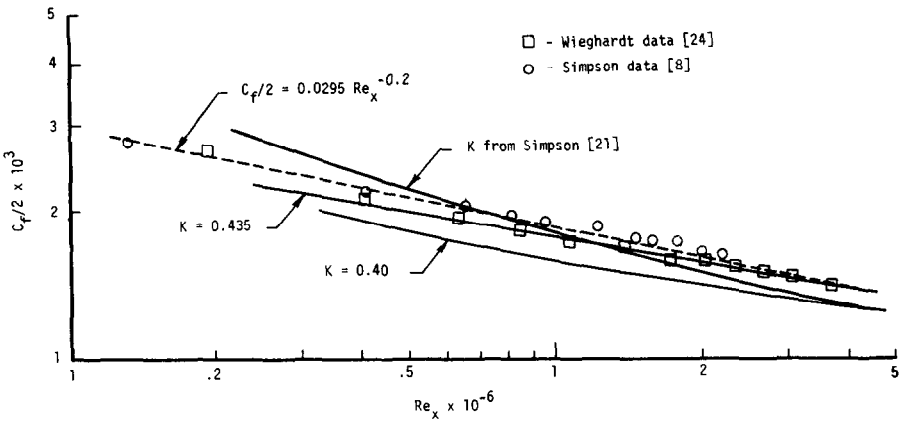

FIG. 1a. Skin friction coefficient: comparison of predictions for various values of K with data for constant property unblown flows.

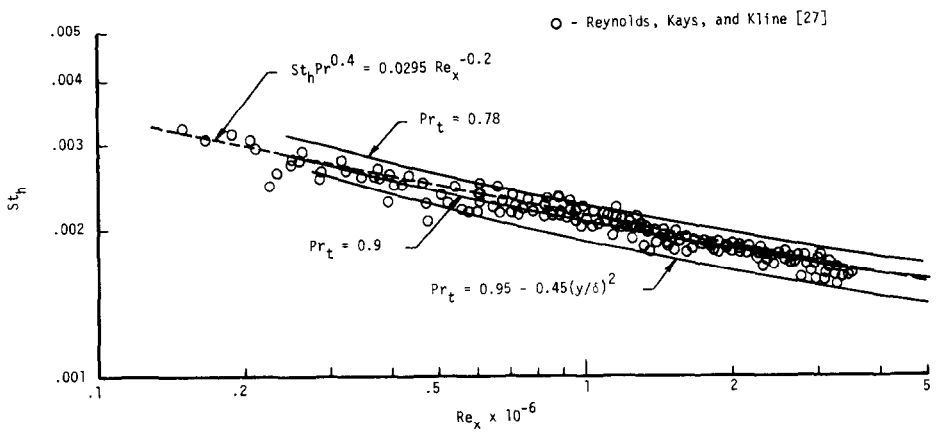

FIG. 1b. Heat transfer Stanton number: comparison of predictions for various values of Pr, with the constant property unblown data of Reynolds, Kays and Kline [27].

data of Wieghardt [24] and Simpson [8] in Fig. 1a shows best agreement for $K = 0{\cdot}435$. Use of $K = 0{\cdot}4$ underpredicts shear stress by about 15 per cent, while Simpson's prescription gives an unacceptable trend with Re_x, overpredicting at small Re_x and underpredicting for $Re_x > 10^6$. Computed values of the shape factor and momentum thickness with $K = 0{\cdot}435$ were found to be in excellent agreement with Wieghardt's data [11].

Models for Pr_t *and* Sc_t

In [11] is an evaluation of the literature on the turbulent Prandtl number, including the recent studies of Blom [25], and Simpson *et al.* [26]. Of particular significance is that Simpson's data shows no discernible effect of blowing rate on Pr_t; thus unblown experimental data for Pr_t can be used to establish a model valid for the calculation of blown boundary layers. Calculations of unblown heat transfer data were made with various constant values of Pr_t, and with the expression, proposed by Simpson for the outer region, $Pr_t = 0{\cdot}95 - 0{\cdot}45(y/\delta)^2$, and which lies within the uncertainty envelope across the entire layer [11]. Comparisons with the incompressible heat transfer data of Reynolds, Kays and Kline [27] are shown in Fig. 1b. A value of $Pr_t = 0{\cdot}9$ gives good agreement with the data; higher values, including Simpson's relation, underpredict the heat transfer rate.

The only experimental data for the turbulent Schmidt number measured in an actual boundary layer flow were reported recently by Dunbar and Squire [28]. Although the results showed some dependence on both shear stress and blowing rate, a constant value of $Sc_t = 0{\cdot}8$ gave reasonable agreement with the data in the fully turbulent inner region. Further, a value of $Sc_t = 1{\cdot}0$ showed poor agreement with the data. Measurements of Sc_t made in the core of turbulent tube flow show considerable disagreement [29, 30], nevertheless a value of $Sc_t = 0{\cdot}8$ is not inconsistent with the data. In our calculations of foreign gas injection there proves to be a ten fold variation in the molecular Schmidt number; the inability of the available data to reliably indicate a dependence of Sc_t on its molecular counterpart is unfortunate, for such a dependence must be expected. The corresponding dilemma for Pr_t is of less consequence since the range of molecular Prandtl numbers encountered is comparatively small.

Selection of the eddy diffusivity model

For constant property flow, calculations were carried out with each of the ε_M models described above, at blowing rates chosen to facilitate comparison with the experimental shear stress data of Simpson *et al.* [8], and the heat transfer data of Moffat and Kays [10]. A detailed evaluation of the models may be found in [11], where it is shown that the Cebeci model probably gives best overall agreement with experiment (with the modification that $K = 0{\cdot}435$ rather than $K = 0{\cdot}4$ as recommended by Cebeci). The Patankar–Spalding model overestimated the reduction in shear at high blowing rates due to excessive damping near the wall ($y^+ < 10$), as could be seen from the associated ε_M profiles. Since all the models are essentially empirical, this suggests that improved agreement may be obtained by adjusting the degree of damping. The Cebeci model is convenient for this purpose; equation (20) rearranged is

$$DF = 1 - \exp\left[-\frac{y^+}{26}(\exp v_s^+)^{y_a^+/2}\right] \quad (23)$$

which clearly shows the role played by the choice of a value for y_a^+ in determining the degree of damping. Further calculations were performed in which y_a^+, now viewed simply as an empirical constant, was varied parametrically; the results are shown in Figs. 2a and 2b. A value of $y_a^+ = 10$ was chosen as giving best agreement with experiment. The relations chosen for parametric calculations of compressible boundary layers with foreign gas injection were therefore

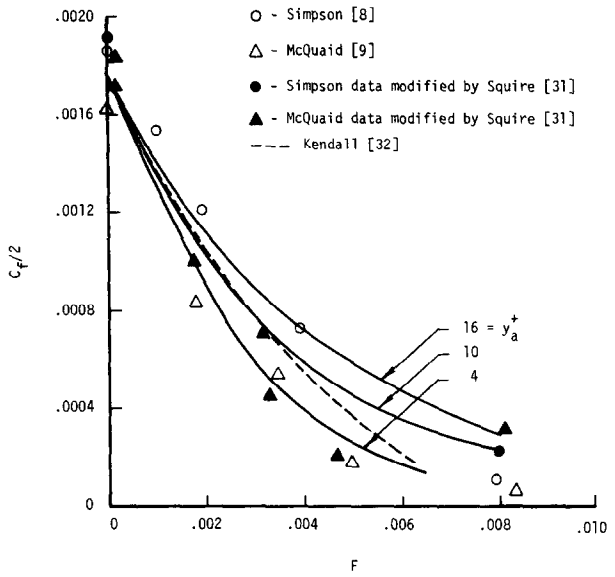

FIG. 2a. Skin friction coefficient: comparison of predictions for various exponents in the damping factor model with constant property blown data. $Re_x = 10^6$; $K = 0{\cdot}435$.

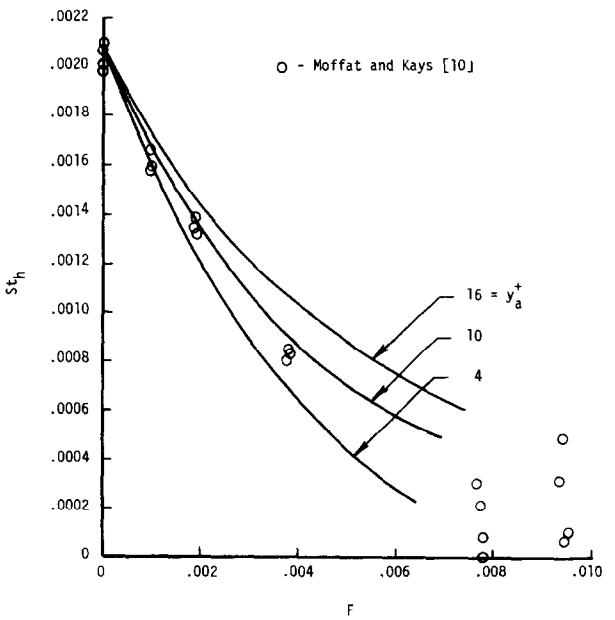

FIG. 2b. Heat transfer Stanton number: comparison of predictions for various exponents in the damping factor model with constant property data of Moffat and Kays [10]. $Re_x = 10^6$; $K = 0{\cdot}435$; $Pr_t = 0{\cdot}9$.

$$\mu_{\text{eff}}|_{\text{inner}} = \mu + \rho(0{\cdot}435y)^2 \left\{1 - \exp\left[-\frac{y^+}{26}(\exp v_s^+)^5\right]\right\}^2 \left|\frac{du}{dy}\right| \quad (24)$$

$$\mu_{\text{eff}}|_{\text{outer}} = \mu + \rho\left\{\frac{K}{4}\delta\left[1 - \exp\left(-\frac{4y}{\delta}\right)\right]\right\}^2 \left|\frac{du}{dy}\right| \quad (25)$$

$$Sc_t = 0{\cdot}8; \quad Pr_t = 0{\cdot}9. \quad (26)$$

RESULTS AND DISCUSSION

Flows calculated

The flows calculated were as follows. For zero Mach number the injectants were H_2, He, CH_4, H_2O, CO, Air, CO_2, Freon 12, Xe and CCl_4, with $T_s/T_e = 0{\cdot}2$ and $0{\cdot}9$. Calculations were also made for synthetic injectants fabricated from CCl_4 and Freon 12 by setting, in turn, their Lennard-Jones parameters, and specific heats equal to those of Xe. The effects of the various problem parameters were studied for He, Air and Xe, (i) in order to study the effect of temperature ratio additional results were obtained for $T_s/T_e = 2{\cdot}0$, (ii) the effect of temperature level was evaluated by obtaining $T_s/T_e = 0{\cdot}9$ as both 295 K/324 K and 1325 K/1472 K, (iii) the effect of Mach number was obtained with data at $M = 2{\cdot}0$ and 6 for $T_s/T_e = 2{\cdot}0$, (iv) the performance of the Patankar–Spalding model was evaluated at $T_s/T_e = 0{\cdot}2$, $M = 0$, and (v) all the above cases were calculated up to $Re_x = 10^6$; the effect of Reynolds number was obtained at $T_s/T_e = 0{\cdot}2$, $M = 0$ by calculating as far as $Re_x = 10^8$. Finally, the effect of a self-similar injection distribution was studied for air at $T_s/T_e = 0{\cdot}2$, $M = 0$, with $\dot{m} \propto x^{-0{\cdot}2}$. For all cases calculations were made at four or more injection rates; in all over 200 marching calculations were made. Complete tabulations of Re_θ, $C_f/2$, St_m, St_h, $m_{1,s}$, ρ_s, Sc_s and Pr_s may be found in [11].

Zero mass injection results

Data for $C_f/2$, St_m and St_h are conveniently presented normalized by corresponding unblown values. In order to recover actual values, values for the zero injection case must be available. In practice such data may be obtained from standard correlations; however, to enable recovery of the exact data calculated in the present study, we present our unblown results. Figures 3a, b and c show, respectively, $C_f^*/2$, St_m^* and St_h^* as a function of Re_x for the temperature ratios and Mach numbers considered. In addition, Fig. 4 shows the Reynolds analogy factor for mass transfer, $2St_m^*/C_f^*$, as a function

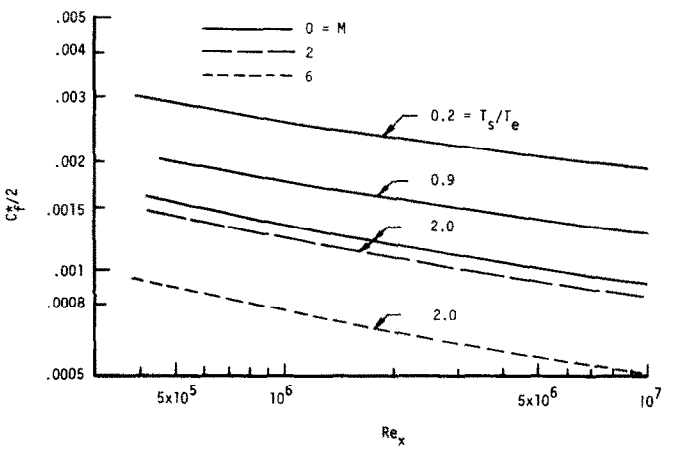

FIG. 3a. Zero mass injection skin friction coefficient as a function of Reynolds number: effect of temperature ratio and Mach number.

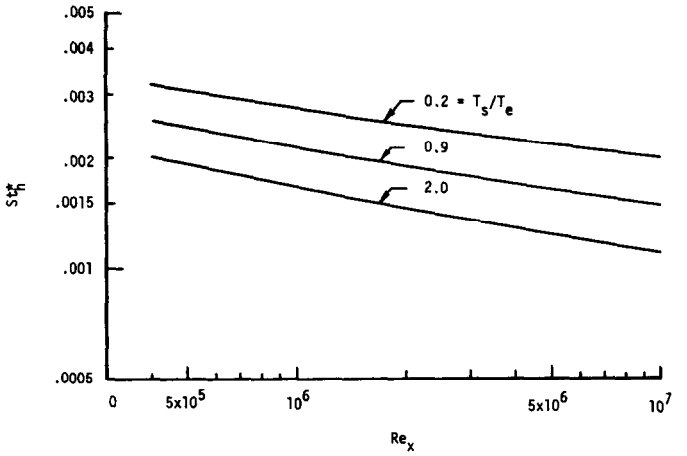

FIG. 3b. Zero mass injection heat transfer Stanton number as a function of Reynolds number: effect of temperature ratio.

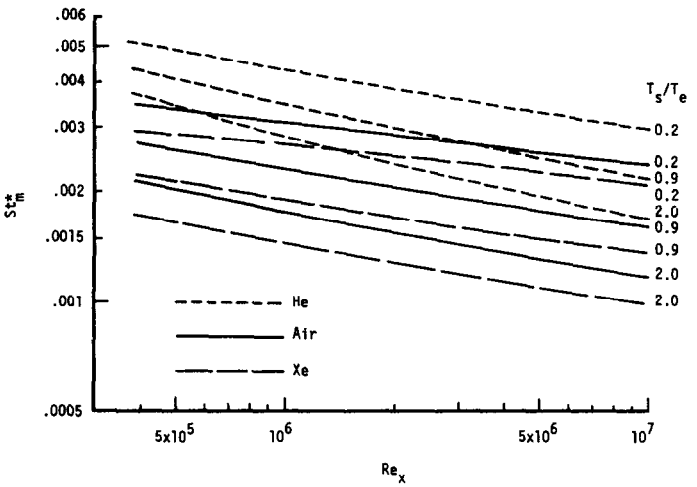

FIG. 3c. Zero mass injection mass transfer Stanton number as a function of Reynolds number: effect of temperature ratio for He, Air and Xe.

of Schmidt number; also in Fig. 4 are shown results for the often used unity turbulent Schmidt number. The essential features of the unblown model, namely $K = 0{\cdot}435$, the van Driest damping factor, and $Pr_t = 0{\cdot}9$ have seen wide use for compressible turbulent boundary layers. We are not concerned here with a detailed evaluation of validity over the range of temperature ratio and Mach number, studies such as those of [33–35], indicate that our predictions of $C_f^*/2$ and St_h^* will compare satisfactorily with experimental data. Other workers undoubtedly prefer slightly different models and, with the current availability of turbulent boundary layer computer programs, will choose to calculate their own unblown data.

Features of the unblown data of relevance to the results for foreign gas injection are as

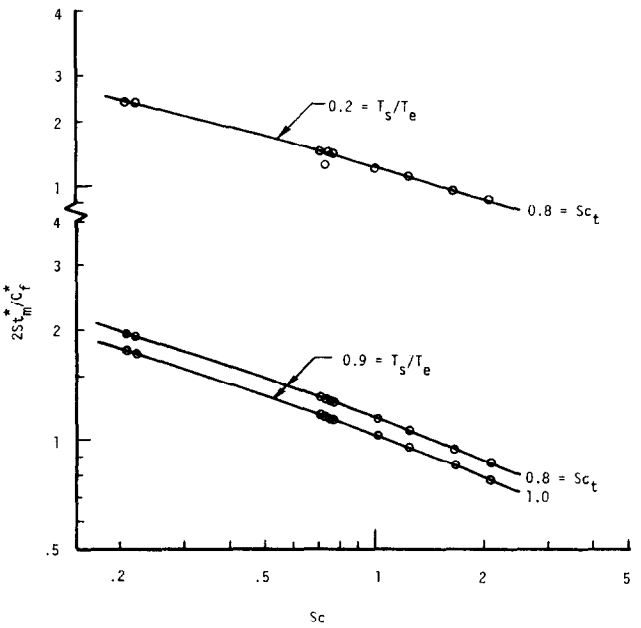

FIG. 4. Zero mass injection Reynolds analogy factor for mass transfer as a function of molecular Schmidt number. (The species associated with each data point may be determined using the values of Sc in Table 1.)

follows. For the range of temperature ratios under consideration, the dependence of $C_f^*/2$ and St_h^* on T_s/T_e is described by

$$C_f^*/2 \propto (T_s/T_e)^{-n}, \quad 0{\cdot}24 < n < 0{\cdot}42 \quad (27)$$

$$St_h^* \propto (T_s/T_e)^{-n}, \quad 0{\cdot}17 < n < 0{\cdot}36. \quad (28)$$

For $M = 0$, the Reynolds analogy factor for mass transfer is adequately correlated as

$$2St_m^*/C_f^* = Sc^{-n}, \quad n = 0{\cdot}28 \text{ for } T_s/T_e = 0{\cdot}2$$
$$= 0{\cdot}36 \text{ for } T_s/T_e = 0{\cdot}9. \quad (29)$$

Effect of injected species

Figures 5a, b and c show, respectively, the skin friction coefficient, the mass transfer Stanton number, and the heat transfer Stanton number, each normalized by their respective unblown values, at zero Mach number for "cold wall" conditions, $T_s/T_e = 0{\cdot}2$. Figures 6a, b and c show corresponding plots for $T_s/T_e = 0{\cdot}9$. The main features of these results may be explained in a manner similar to which characteristics of binary laminar boundary layers were assessed in [36–38].

The general manner in which injection of a like species into a boundary layer (e.g. air into air) reduces skin friction is clearly shown by constant property solutions. Foreign gas injection yields reductions different to those obtained for like species injection resulting from the effects of composition on mixture transport and thermodynamic properties. Despite the complex coupling of the conservation equations due to property variations, it is possible to identify primary effects and thereby explain the trends exhibited by the data. Physical property variations influence the momentum equation only through the product $\rho\mu_{\text{eff}}$ (or equivalently $C_{\text{eff}} = \rho\mu_{\text{eff}}/\rho_e\mu_e$) as can be seen upon examination of equation (9). The same observation applies to laminar boundary layers, as can be easily seen from the conventional transformed momentum equation, e.g. Lees [39]. The effect

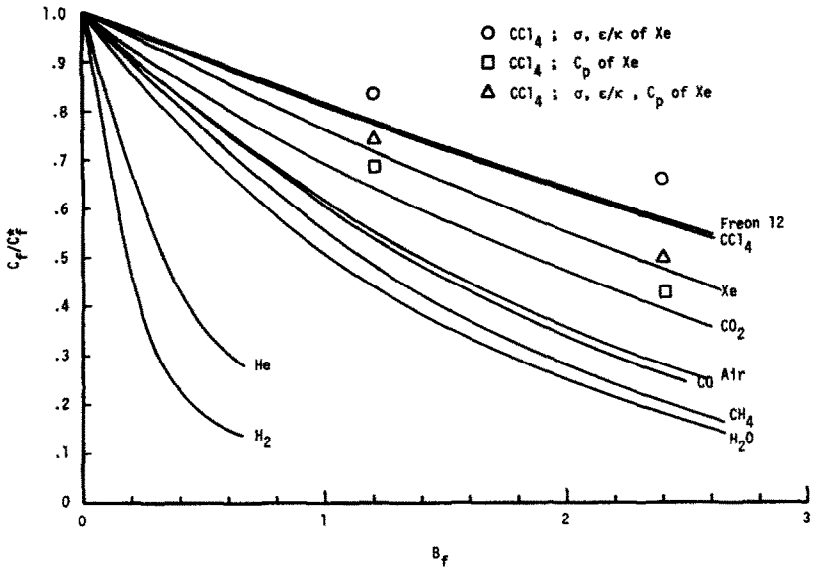

FIG. 5a. Effect of injection on skin friction. $M=0, T_s/T_e=0{\cdot}2$.

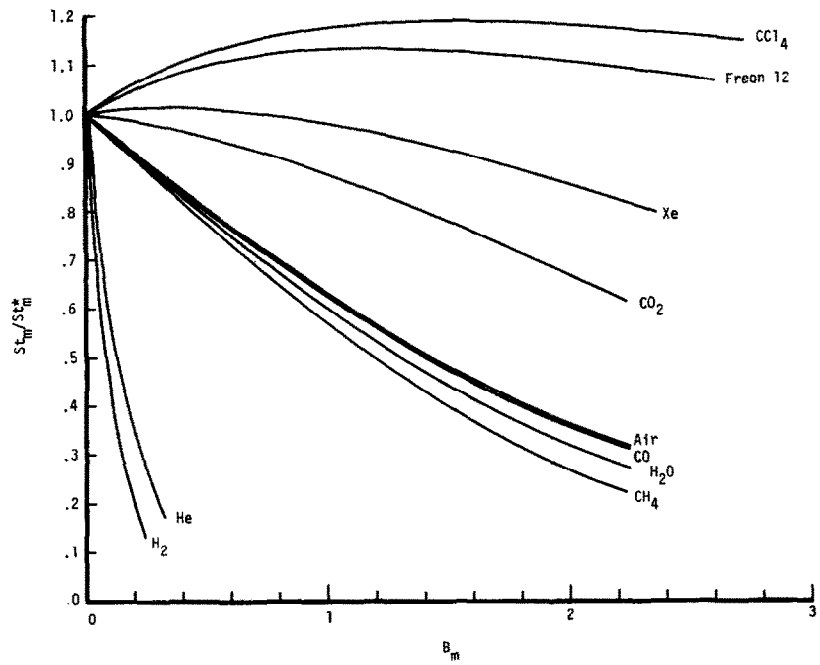

FIG. 5b. Effect of injection on the mass transfer Stanton number. $M = 0$, $T_s/T_e = 0{\cdot}2$.

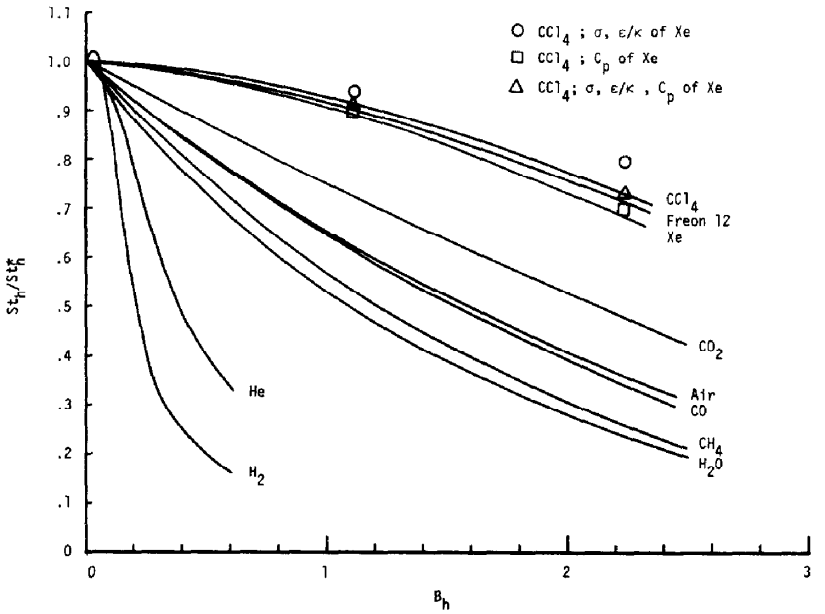

FIG. 5c. Effect of injection on heat transfer. $M=0$, $T_s/T_e=0{\cdot}2$.

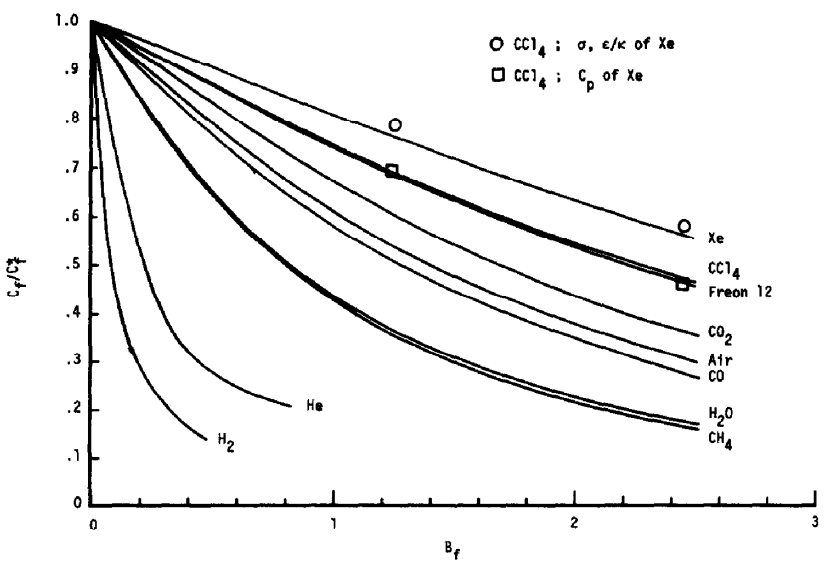

FIG. 6a. Effect of injection on skin friction. $M=0$, $T_s/T_e=0{\cdot}9$.

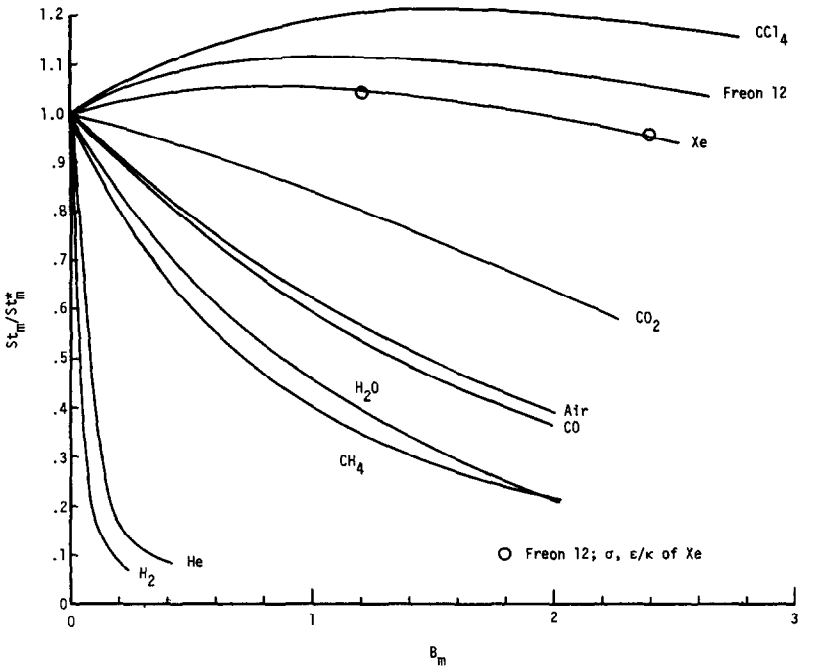

FIG. 6b. Effect of injection on the mass transfer Stanton number. $M = 0$, $T_s/T_e = 0{\cdot}9$.

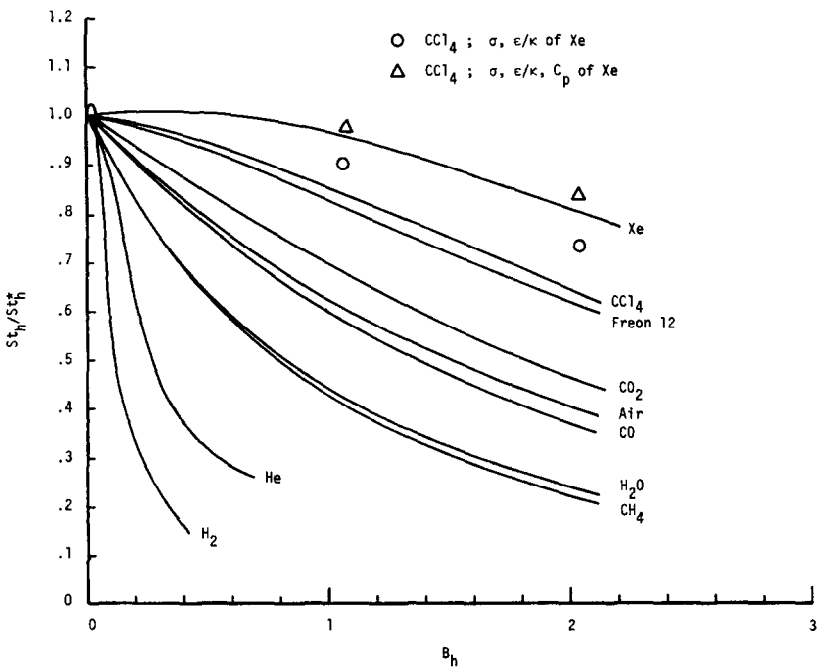

FIG. 6c. Effect of injection on heat transfer. $M = 0$, $T_s/T_e = 0{\cdot}9$.

of foreign gas injection is quite similar to the effect of change in wall temperature on an unblown compressible boundary layer. Density is directly proportional to molecular weight; molecular viscosity tends to increase weakly, but very irregularly, with molecular weight, as can be seen from the data in Table 1. However the turbulent contribution to μ_{eff} is proportional to local density so that the product $\rho\mu_{\text{eff}}$ will depend very regularly on molecular weight in the logarithmic region of the law of the wall. Since it is this region which mostly determines the wall shear stress, $C_f/2$ should be expected to be a regular function of molecular weight. Figures 5a and 6a show that, except for the very heavy injectants, the effectiveness does indeed vary regularly with molecular weight. The heavy species Freon 12, Xe and CCl_4 have relatively close molecular weights; as we shall demonstrate later when we discuss the results for the synthetic injectants, the anomalous behavior for the heavy injectants is due to large differences in specific heats and molecular viscosities. In comparison with laminar boundary layers, the effectiveness is more strongly dependent on molecular weight. The above mentioned analogy with the response of an unblown boundary layer to changes in wall temperature confirms that this feature is not unexpected. In the previous section we showed, for a turbulent air boundary layer, that $C_f^*/2 \propto (T_s/T_e)^{-0.3}$ approximately; for a laminar air boundary layer it is well known that $C_f^*/2 \propto C_{\text{eff. s}}^{0.1}$, i.e. approximately proportional to $(T_s/T_e)^{-0.025}$. The stronger dependence on (T_s/T_e) for the turbulent case is due to the more important role played by density variations, and immediately suggests a stronger dependence on injectant molecular weight for foreign gas injection.

Turning now to the mass transfer Stanton number, the trends shown by the results in Figs. 5b and 6b are most easily explained via the Reynolds analogy factor and the already described skin friction behavior. The effective Schmidt number is a measure of the relative rates of momentum and species transport. Since the results are normalized with St_m^*, we are interested in how Sc_{eff} varies as the foreign gas is injected. Not too far from the wall Sc_{eff} becomes equal to $Sc_t = 0{\cdot}8$; but the major resistance to mass transfer is near the wall where the molecular Schmidt number plays an important role. Thus the main features of Figs. 5b and 6b can be explained in terms of the effect of properties on $Sc = \mu/\rho\mathscr{D}_{12}$. The binary diffusion coefficient is composition independent; with increasing injectant molecular weight Sc decreases through ρ, with a weak and irregular counteracting trend through μ. However, account must be taken of the fact that mixture thermodynamic properties vary with the mass fractions of the components, whereas mixture transport properties vary with mole fractions. For a given mass injection rate the wall mole fraction $x_{1.s}$ is typically much larger for a light injectant than for a heavy one. Thus the viscosity of a light injectant will have a greater effect on Sc than will a heavy one. The primary C_{eff} effect identified for skin friction is strongly augmented by a Sc_{eff} effect, which is mostly a density effect. Figures 5b and 6b confirm this assessment; not only is St_M/St_m^* more strongly dependent on injectant molecular weight than is C_f/C_f^*; for the three heaviest injectants, Freon 12, Xe and CCl_4, St_m/St_m^* increases above unity, and very high blowing rates are required to obtain a reduction below unity. Discussion of the anomalous behavior for Freon 12 will be deferred until the results for synthetic injectants are introduced. For laminar boundary layers these increases in the mass transfer Stanton number for heavy injectants are not obtained [38], which emphasizes the important effect of density variation through C_{eff}.

With regards to heat transfer, the trends shown by the results in Figs. 5c and 6c are also best explained via the Reynolds analogy factor and the already described skin friction behavior. The effective Prandtl number is a measure of the relative rates of momentum and energy transport. Away from the wall Pr_{eff} becomes

heat transfer is near the wall where molecular Prandtl number plays a dominant role. Thus the main features of the figures can be explained by the effect of properties on $Pr = C_p\mu/k$. Both k and C_p decrease with increasing molecular weight, but C_p more strongly so; in addition C_p increases with the complexity of the molecule. The weak and irregular increase of μ with molecular weight has rather less effect on Pr. The transport property k plays a more important role for light injectants owing to the large values of $x_{1.s}$ which typically prevail. Thus the effect of Pr_{eff} is to augment the primary C_{eff} effect, but not as strongly as was the case for Sc_{eff}. The results in Figs. 5c and 6c confirm this line of reasoning. Again there is anomalous behavior for the heavy injectants, which will be discussed later. The initial increase in St_h for H_2, and the inflection in the He curve, are due to the high thermal conductivity of these light injectants, a feature first noted by Rubesin and Pappas [4]. At low blowing rates the mixture conductivity near the wall increases more rapidly than the specific heat because of the characteristically large value of the mole fraction $x_{1.s}$ for light injectants; an increase in heat transfer results. At high blowing rates the effects of C_p and C_{eff}, which are both dependent on mass fraction, dominate to yield the large reductions in heat transfer typical of light gas injection. The inflection in the He curve is less pronounced than that found for laminar flow [38], again emphasizing the important effect of density variation through C_{eff}.

In order to clarify the anomalous behavior for the heavy injectants Freon 12, Xe and CCl_4, calculations were made for synthetic injectants fabricated from CCl_4 and Freon 12 by setting, in turn, their Lennard–Jones parameters and specific heats equal to those for Xe. Since the molecular weights of Freon 12 and CCl_4 are close to the values for Xe, equating Lennard–Jones parameters leads to almost identical species viscosities. The results are shown in Figs. 5 and 6; we offer the following observations,

(i) Figure 6a: for a nearly isothermal boundary layer ($T_s/T_e = 0{\cdot}9$), changing C_p for CCl_4 has negligible effect on C_f/C_f^*, but giving CCl_4 the viscosity of Xe moves C_f/C_f^* to be a little higher than the Xe curve, consistent with the remaining molecular weight effect.

(ii) Figure 5a: for cold wall conditions ($T_s/T_e = 0{\cdot}2$), changing the viscosity of CCl_4 to that of Xe again significantly increases C_f/C_f^*, but away from the Xe curve. Changing C_p dramatically decreases C_f/C_f^*. The lower specific heat corresponding to Xe causes higher temperatures through the boundary layer; the lower density and associated poorer turbulent transport result in decreased skin friction. On changing both μ and C_p, C_f/C_f^* moves to be a little higher than the Xe curve, again consistent with the remaining molecular weight effect.

(iii) Figure 6b: changing the viscosity of Freon 12 lowers the value of St_m/St_m^* to be about equal to that for Xe. Thus the anomalous mass transfer behavior of Freon 12 is essentially due to its viscosity.

(iv) Figure 6c: for a nearly isothermal boundary layer, changing the Lennard–Jones parameters for CCl_4 moves St_h/St_h^* upwards, closer to the Xe curve; however the effect of the higher C_p of CCl_4 remains. If, in addition, C_p is changed, then St_h/St_h^* assumes values consistent with the remaining molecular weight effect.

(v) Figure 5c: for cold wall conditions, decreasing C_p of CCl_4 to the value for Xe, lowers the value of St_h/St_h^*, a phenomenon which could never occur for a laminar boundary layer. The direct effect of C_p is through the Prandtl number, a lower value of C_p lowers Pr and hence increases the Reynolds analogy factor. But we see here that the opposing effect of a lower C_p in increasing temperature and density in the boundary layer, decreases the turbulent transport sufficient to outweigh the direct C_p effect.

Effect of temperature ratio

Figures 7a, b and c show the effects of T_s/T_e on, respectively, $C_f/2$, St_m and St_h. The abscissas are the conventional blowing parameters,

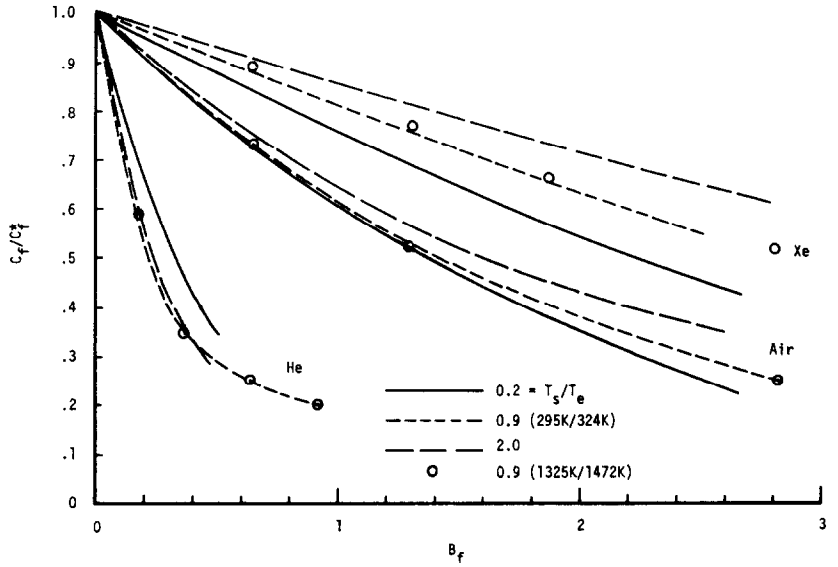

FIG. 7a. Effect of temperature ratio and temperature level on skin friction reduction. He, Air and Xe at $M = 0$.

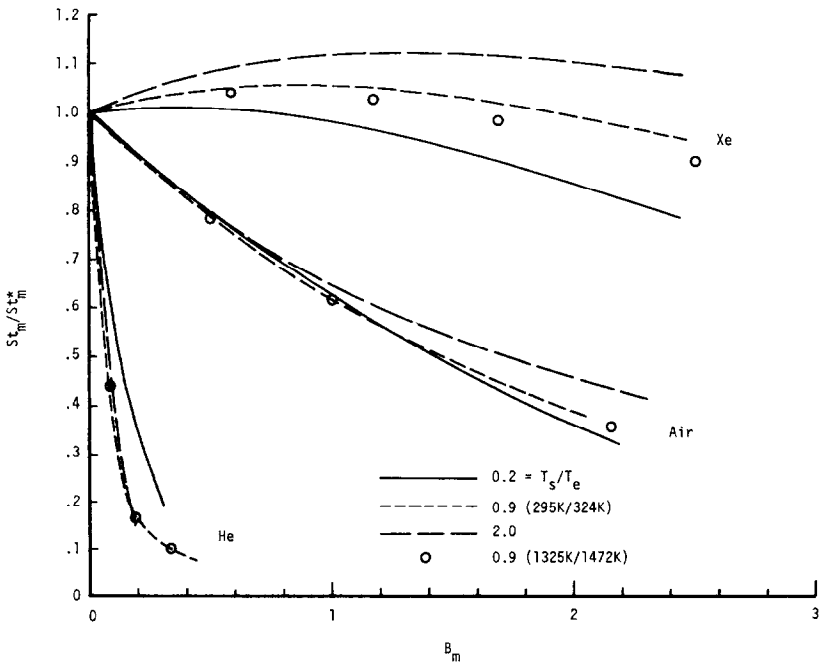

FIG. 7b. Effect of temperature ratio and temperature level on mass transfer Stanton number reduction. He, Air and Xe at $M = 0$.

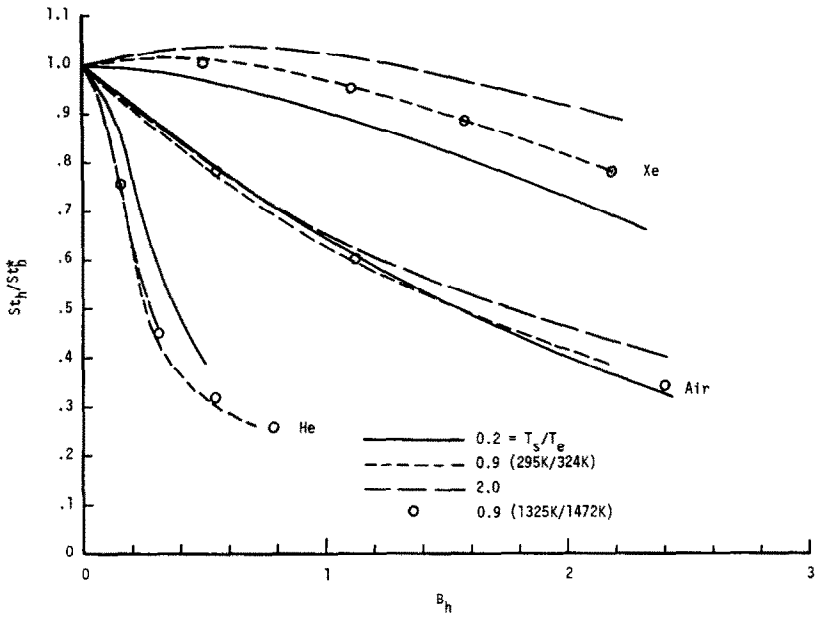

FIG. 7c. Effect of temperature ratio and temperature level on heat transfer reduction. He, Air and Xe at $M = 0$.

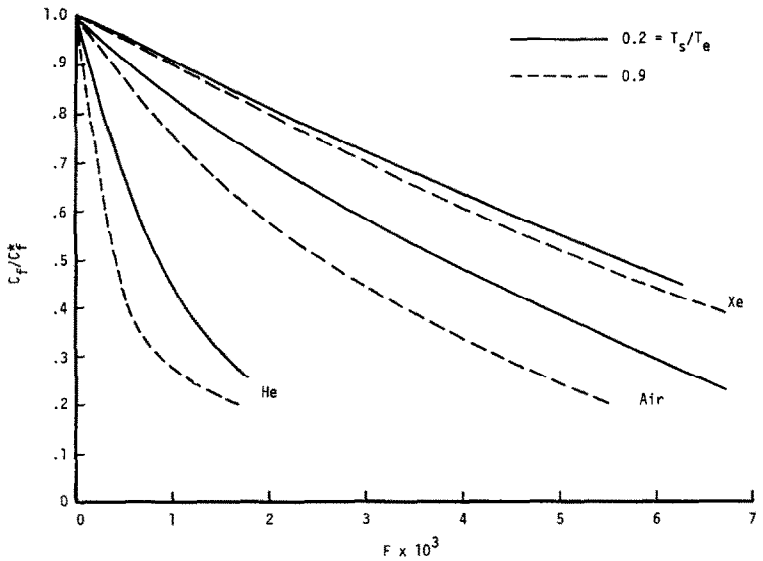

FIG. 8. Effect of temperature ratio on skin friction reduction: C_f/C_f^* as a function of F at $M = 0$.

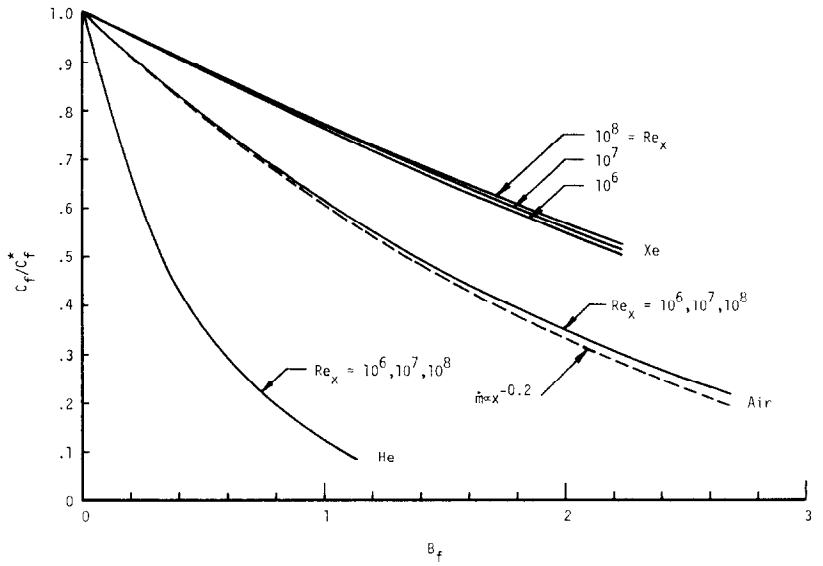

FIG. 9. Effect of Reynolds number and injection distribution on skin friction reduction. $M = 0$, $T_s/T_e = 0{\cdot}2$.

respectively, B_f, B_m and B_h. Before discussing the trends displayed in Figs. 7, it will be instructive to consider in detail the significance of the use of say, B_f, as an appropriate abscissa. Recall that in Fig. 5a, the value of $C_f^*/2$ used to form $B_f = 2F/C_f^*$ was the same for all injectants, since T_s/T_e, M and Re_x were fixed; thus the abscissa was simply a constant times $\dot{m}$, and features of the curves were explained in terms of expected effects for a given mass injection rate. More generally, scaling F with $C_f^*/2$ will, for a self-similar flow, eliminate the effect of Re_x. For laminar self-similar flows this objective is often attained by using, as abscissa, the dimensionless stream function $-f_s$, which is already scaled by the appropriate Reynolds number function [38]. For flat plate turbulent flows an injection distribution $\dot{m} \propto x^{-0{\cdot}2}$ yields an essentially self-similar flow, and a scaling of F with $C_f^*/2$, which contains the appropriate Reynolds number function $Re_x^{-0{\cdot}2}$, completely eliminates the Re_x dependence. For constant $\dot{m}$ the flow is nonsimilar and, as is shown in Fig. 9, a small residual Re_x effect remains.

In Fig. 7a, $C_f^*/2$ differs for the solid curves because of differing wall temperatures; Re_x is the same for each curve. Thus the curves do not collapse onto each other, and also the abscissa is no longer only proportional to $\dot{m}$. Figure 8 shows C_f/C_f^* plotted against simply $F = \dot{m}/\rho_e u_e$ which, for fixed free stream conditions, is a constant times $\dot{m}$. When plotted in this manner the trends shown by the results are easy to explain. Equation (27) shows that $C_f^*/2$ is approximately proportional to $(T_s/T_e)^{-0{\cdot}3}$, i.e. increased wall temperatures lead to lower values of $C_f^*/2$, primarily due to the reduced density. Normalization with the unblown value does not completely remove the effect of (T_s/T_e) from C_f/C_f^* due to the distortion of the C_{eff} profile by mass transfer; the flattening of the temperature profile near the wall extends the influence of the wall temperature further into the boundary layer. By this reasoning C_f/C_f^* should decrease with increasing wall temperature, as is borne out by the curves in Fig. 8. Returning now to Fig. 7a, the objective behind using B_f is twofold, (i) to have the results in a more convenient form for engineering calculations, and (ii) to attempt to further reduce the

effect of the problem parameter T_s/T_e. By scaling F with $2/C_f^*$ we are using C_f^* a second time (the first was to normalize C_f), now to attempt removal of the residual effect of T_s/T_e due to distortion of the C_{eff} profile. Such a scaling must always tend to move the curves towards each other, but over-corrections and non-monotonic behavior can result. Figure 7a shows such over-corrections for air and Xe, and a somewhat irregular behavior for He.

Similar arguments to those made above for skin friction can be made with regards to the mass and heat transfer Stanton numbers. Thus the nonmonotonic behavior of the air results in Figs. 7b and c is not unexpected, and also shows that the scaling of F for these cases is reasonably appropriate. Of particular interest is the gross over-correction for Xe injection in all of Figs. 7a, b and c. Jeromin [1] presents experimental data for heavy gas injection (Freon 12) in the form of plots similar to Figs. 7a and c, but failed to attempt an isolation of temperature ratio as a parameter; thereby diminishing the value of the plots.

Figures 7a, b and c also show the effect of temperature level since calculations at $T_s/T_e = 0{\cdot}9$ were made for both 295 K/324 K and 1325 K/1472 K. The effect is clearly very small. The normalization with the zero blowing value and the scaling in the blowing parameter is quite successful in eliminating the temperature level dependence introduced by variable species specific heats and the Lennard–Jones potential model.

Effect of Reynolds number and injection distribution

In Fig. 9 is shown the effect of Reynolds number on skin friction at $M = 0$, $T_s/T_e = 0{\cdot}2$, for $Re_x = 10^6$, 10^7 *and* 10^8. The effect is seen to be small relative to the effects of the parameters already discussed, and is negligible for practical purposes. Its source is the weakly nonsimilar blowing, as $\dot{m}$ has been held constant independent of x. For a flat plate turbulent boundary layer an approximately self-similar flow is obtained for $\dot{m} \propto x^{-0.2}$; calculations performed for such a distribution indicate a

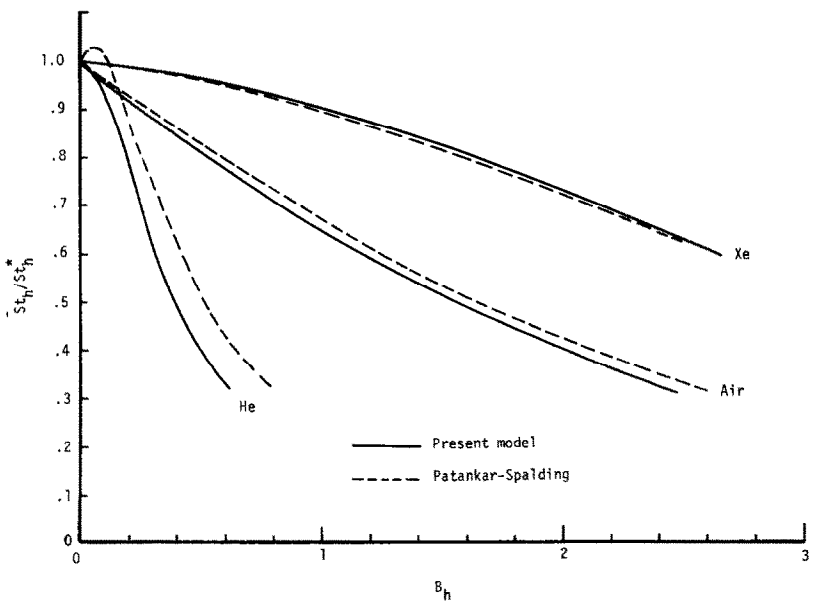

FIG. 10. Effect of eddy diffusivity model on heat transfer reduction. $M = 0$, $T_s/T_e = 0{\cdot}2$.

complete elimination of the Reynolds number dependence. Our results contradict the predictions of the analyses of Rubesin and Pappas [4], and Kendall [32], where a significant Re_x effect was found for constant $\dot{m}$. We conclude that the Re_x effect found by these latter analyses is an error due to the use of Couette forms of the conservation equations; our use of an exact solution procedure for the governing differential equations has avoided such an error.

Associated with the effect of Reynolds number, is the effect of injectant distribution. As would be expected from the above discussion of the Re_x effect, the calculations made for $\dot{m} \propto x^{-0.2}$ yield curves of C_f/C_f^*, St_m/St_m^* and St_h/St_h^* which are very little different to those for $\dot{m} =$ constant. Thus for engineering purposes no distinction need be made between constant blowing and self-similar blowing.

Effect of turbulent transport models

Figure 10 shows, for heat transfer, the effect of inner region eddy diffusivity model with He, Air and Xe injection at $M = 0$, $T_s/T_e = 0{\cdot}2$. These results are included to demonstrate that the normalized form St_h/St_h^* when plotted against B_h is relatively insensitive to the choice of inner region eddy diffusivity model. The most significant discrepancy is seen for He injection, and is due to the sensitivity of the damping factor to density variations. For the skin friction coefficient and mass transfer Stanton number, similar conclusions may be drawn [11]. Thus the discrepancies between the predictions of the Patankar–Spalding model, and the model we have used are small enough to be of no consequence to our discussions of the effects of foreign gas injection.

Comparisons with experiment for low speed flow

Figures 11 and 12 show comparisons of the $M = 0$, $T_s/T_e = 0{\cdot}9$ predictions with experimental data, for He and Freon 12 injection into low speed air flow. Details of the experimental studies have been compiled by Jeromin [1]; the parameters T_s/T_e, Re_x and M do vary somewhat, but not sufficiently to affect our conclusions. All the available data for skin

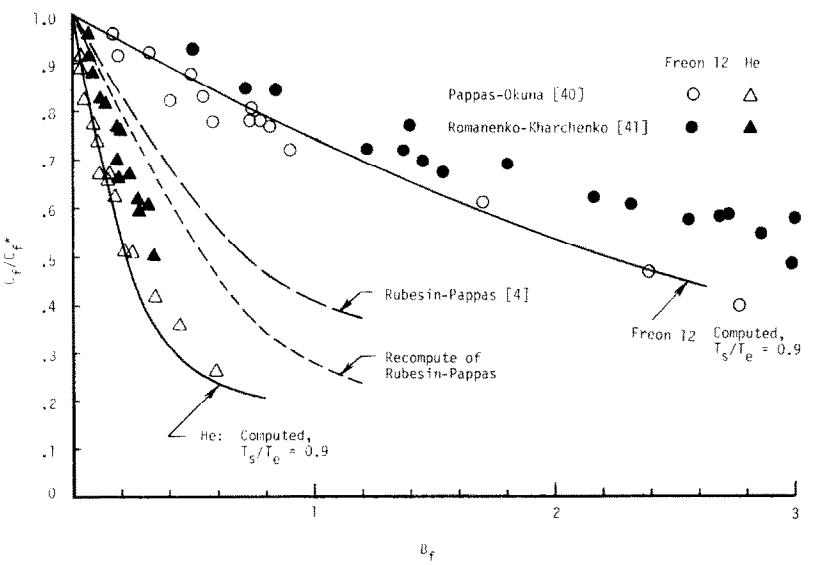

FIG. 11. Comparison of predicted skin friction with experimental data for low speed flows.

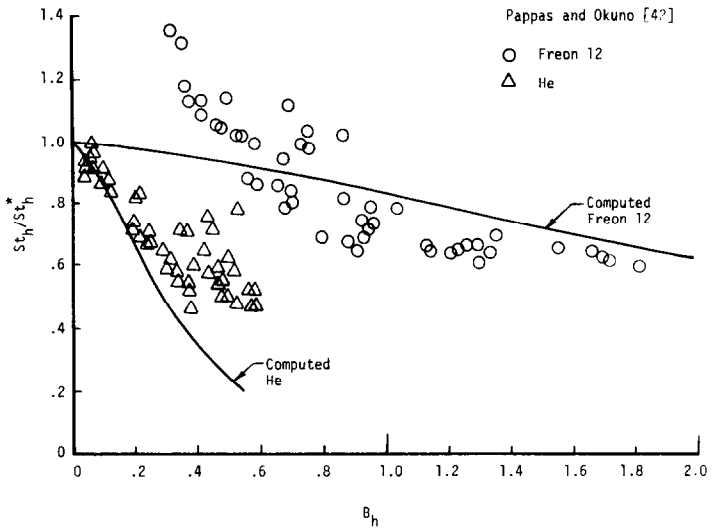

FIG. 12. Comparison of predicted heat transfer with experimental data for low speed flows.

friction are shown in Fig. 11; the predictions agree well with Pappas and Okuno [40], but fall below Romanenko and Kharchenko [41]. Also of interest is the prediction for He injection of Rubesin and Pappas [4], since their curve lies above the experimental data. Rubesin and Pappas evaluated the integrals in their equations (67) and (76) by approximate analysis; using exact numerical quadrature we obtained lower values of C_f/C_f^*, as shown in Fig. 11. This relative insensitivity of the Rubesin–Pappas model to density variations is due mostly to injection increasing the thickness of the laminar sub-layer.

In Fig. 12 we have not shown the heat transfer data of Romanenko and Kharchenko [41], since we are unclear as to the correct interpretation of their blowing parameter (see also Tewfik [42]). The predictions of St_h/St_h^* agree well with the data of Pappas and Okuno [43], but are somewhat low for He. In summary, the comparisons with experiment are satisfactory, though there is perhaps a tendency to underpredict both skin friction and heat transfer for He injection.

Effect of Mach number

Figure 13 shows the predicted effect of Mach number on skin friction at $T_s/T_e = 2{\cdot}0$. The abscissa in Fig. 13 is the conventional $B_f = 2\dot{m}/\rho_e u_e C_f^*$, but for the parameter values under consideration, the behavior of the predictions is most easily explained if an abscissa proportional only to $\dot{m}$ is chosen. Such a graph was found to show no effect of M for air injection, while C_f/C_f^* increased with M for the injection and decreased for Xe injection. Clearly, for air injection, the large effect of M on C_f shown in Fig. 3a is removed by normalization with C_f^*. Based on the above observation the effects of foreign gas injection are easy to explain. Injection of the He lowers μ_{eff} and hence also viscous dissipation. Thus, compared to air injection, temperatures are lower and the counteracting increase of $(\rho\mu)_{\text{eff}}$, through the temperature dependence of ρ, increases the skin friction. Reasoning along the same lines for Xe indicates a decrease in C_f/C_f^* with increasing M for Xe.

In Fig. 14 predictions of skin friction for air injection are compared with the experimental

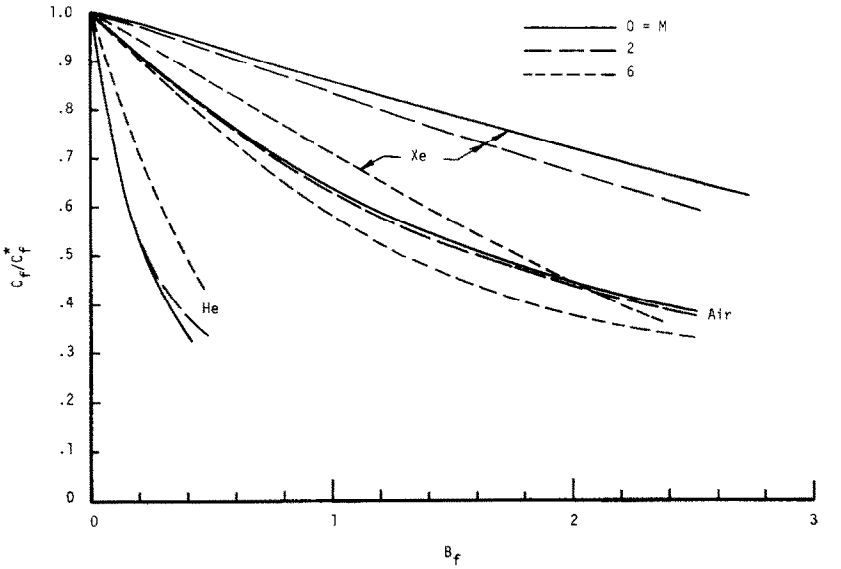

FIG. 13. Predicted effect of Mach number on skin friction reduction at $T_s/T_e = 2{\cdot}0$.

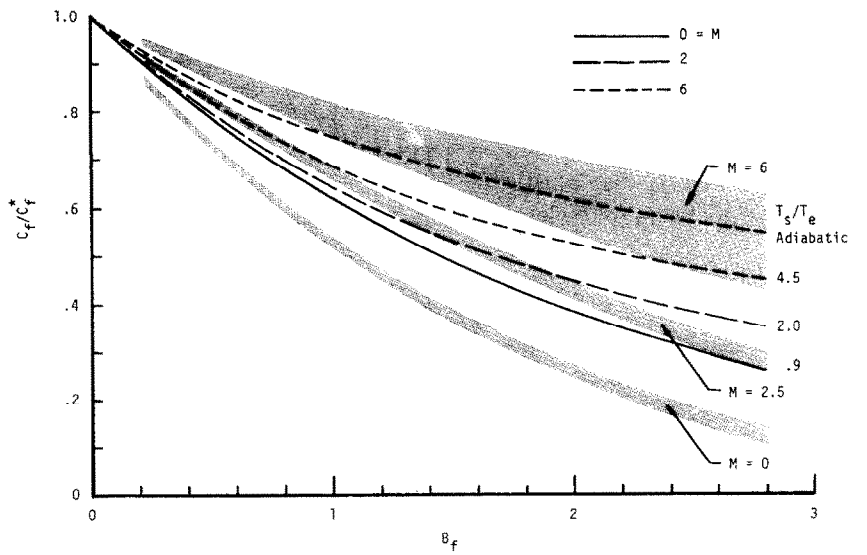

FIG. 14. Comparison of predicted skin friction with experiment for air injection into high speed flows; the data bands are those presented by Jeromin [1].

data bands presented by Jeromin [1]. The large increase in C_f/C_f^* with increasing M shown by the experimental data (in contrast to the decrease in Fig. 13) proves to be primarily an effect of T_s/T_e. An examination of the original data sources indicated that for $M = 0$ a value of $T_s/T_e \cong 0{\cdot}9$ is typical; for $M = 2$, $T_s/T_e \cong 2{\cdot}0$; while for $M = 6$, T_s/T_e might lie between 4·5 and the adiabatic wall value. Figure 14 shows that, when appropriate temperature ratios are used, the predicted effect of Mach number is consistent with experiment. The discrepancy at $M = 0$ is due to Jeromin's reliance on the data of McQuaid (see Fig. 2a). In evaluating the adequacy of the predictions at $M = 6$ it should be noted that there is considerable scatter in Danberg's $M = 6$ data [44]; measurements of C_f/C_f^* varied from 0·5 to 0·8 at the same value of B_f.† In many high Mach number engineering problems, e.g. ablative and transpiration cooling, the wall is relatively cool: our results demonstrate the importance of correctly accounting for the parameter T_s/T_e, and the utility of our finite difference calculation procedure for this purpose.

CONCLUSIONS

1. An efficient finite difference procedure has been developed to calculate compressible turbulent boundary layers on flat plate with foreign gas injection.
2. An eddy diffusivity model has been established which adequately predicts skin friction and heat transfer for constant property air into air injection.
3. Predictions of skin friction and heat transfer for foreign gas injection into low speed flows agree satisfactorily with experiment. The mass and heat transfer Stanton numbers for the heaviest injectants are found to actually initially increase with injection rate. The critical role played by density variations across the boundary layer is clearly shown and explained.
4. The effects of temperature ratio on blown flows can be readily explained in terms of the well established behavior of unblown flows.
5. The predicted effect of Mach number on skin friction agrees satisfactorily with experiment provided the effect of temperature ratio on the data is recognized and accounted for.

† We are grateful to an anonymous reviewer for assistance in clarifying these points.

REFERENCES

1. L. O. F. JEROMIN, The status of research in turbulent boundary layers with fluid injection, *Progress in Aeronautical Sciences*, Vol. 10, edited by D. KUCHEMANN, pp. 65–189. Pergamon Press, Oxford (1970).
2. D. B. SPALDING, D. M. AUSLANDER and T. R. SUNDARAM, The calculation of heat and mass transfer through the turbulent boundary layer on a flat plate at high Mach numbers, with and without chemical reaction, *Supersonic Flow, Chemical Processes and Radiative Transfer*, edited by D. B. OLFE and V. ZAKKAY, pp. 211–276. Pergamon Press, Oxford (1964).
3. N. NESS, Foreign gas injection into a compressible turbulent boundary layer on a flat plate, *J. Aero/Space Sci.* **28**, 645 (1961).
4. M. W. RUBESIN and C. C. PAPPAS, An analysis of the turbulent boundary-layer characteristics on a flat plate with distributed light-gas injection, NACA Technical Note 4149 (1958).
5. S. V. PATANKAR and D. B. SPALDING, *Heat and Mass Transfer in Boundary Layers*. Morgan-Grampian, London (1967).
6. V. E. DENNY and A. F. MILLS, Nonsimilar solutions for laminar film condensation on a vertical surface, *Int. J. Heat Mass Transfer* **12**, 965–979 (1969).
7. V. E. DENNY and R. B. LANDIS, An improved transformation of the Patankar-Spalding type for numerical solution of two-dimensional boundary layer flows, *Int. J. Heat Mass Transfer* **14**, 1859–1862 (1971).
8. R. L. SIMPSON, R. J. MOFFAT and W. M. KAYS, The turbulent boundary layer on a porous plate: experimental skin friction with variable injection and suction, *Int. J. Heat Mass Transfer* **12**, 771–789 (1969).
9. J. MCQUAID, Experiments on incompressible turbulent boundary layers with distributed injection, Aeronautics Research Council Report and Memoranda No. 3549 (January 1967).
10. R. J. MOFFAT and W. M. KAYS, The turbulent boundary layer on a porous plate: experimental heat transfer with uniform blowing and suction, *Int. J. Heat Mass Transfer* **10**, 1547–1566 (1968).
11. R. B. LANDIS, Numerical solution of variable property turbulent boundary layers with foreign gas injection, Ph.D. Dissertation, School of Engineering and Applied Science, University of California, Los Angeles (1971).
12. R. A. SVEHLA, Estimated viscosities and thermal conductivities of gases at high temperatures, NASA Technical Report R132 (1962).

13. *Handbook of Chemistry and Physics, Forty-First Edition*, p. 2289. Chemical Rubber Publishing Co., Cleveland (1959).
14. *JANAF Thermochemical Tables*, edited by E. T. DERGAZARIAN *et al.* The Dow Chemical Co., Midland, Michigan, (1960); and supplements to date.
15. I. W. BUDDENBERG and C. R. WILKE, Viscosities of some mixed gases, *J. Phys. Colloid. Chem.* **55**, 1491–1498 (1951).
16. D. K. EDWARDS, V. E. DENNY and A. F. MILLS, *Transfer Processes*. Holt, Rinehart & Winston, New York (in press).
17. T. CEBECI, Behavior of turbulent flow near a porous wall with pressure gradient, *AIAA Jl* **8**, 2152–2156 (1970).
18. R. B. KINNEY and E. M. SPARROW, Turbulent flow, heat transfer, and mass transfer in a tube with surface suction, *J. Heat Transfer* **92**, 117–125 (1970).
19. T. E. POWELL and A. B. STRONG, Calculation of the two-dimensional turbulent boundary layer with mass addition and heat transfer, *Proceedings of the* 1970 *Heat Transfer and Fluid Mechanics Institute*, pp. 153–166. Stanford University Press, Stanford, California (1970).
20. E. R. VAN DRIEST, On turbulent flow near a wall. *J. Aero Sci.* **23**, 1007–1011 (1956).
21. R. L. SIMPSON, Characteristics of turbulent boundary layers at low Reynolds numers with and without transpiration, *J. Fluid Mech.* **42**, 769–802 (1970).
22. M. P. ESCUDIER, The distribution of the mixing length in turbulent flows near walls, Imperial College, Mechanical Engineering Department, Report TWF/TN/1 (1965).
23. P. S. KLEBANOFF, Characteristics of turbulence in a boundary layer with zero pressure gradient, NACA TN 3178 (July 1954).
24. D. COLES and E. A. HIRST, *Proceedings of the AFOSR-IFP-Stanford Conference on Computation of Turbulent Boundary Layers, Volume II, Compiled Data*, Thermosciences Division, Department of Mechanical Engineering, Stanford University, Stanford, California (1968).
25. J. BLOM, An experimental determination of the turbulent Prandtl number in a developing temperature boundary layer, Thesis, Technological University, Eindhoven, The Netherlands (1970).
26. R. L. SIMPSON, D. G. WHITTEN and R. J. MOFFAT, An experimental study of the turbulent Prandtl number of air with injection and suction, *Int. J. Heat Mass Transfer* **13**, 125–144 (1970).
27. W. C. REYNOLDS, W. M. KAYS and S. J. KLINE, Heat transfer in the turbulent incompressible boundary layer, I—constant wall temperature, NASA Memo 12-1-58W (December 1958).
28. D. I. A. DUNBAR and L. C. SQUIRE, Correlations of concentration, temperature and velocity profiles in compressible turbulent boundary layers with foreign gas injection, *Int. J. Heat Mass Transfer* **14**, 27 40 (1971).
29. N. SHERIFF and D. J. O'KANE, Eddy diffusivity of mass measurements for air in circular ducts, *Int. J. Heat Mass Transfer* **14**, 697–708 (1971).
30. I. B. GOLDMAN and J. M. MARCHELLO, Turbulent Schmidt numbers, *Int. J. Heat Mass Transfer* **12**, 797–802 (1969).
31. L. C. SQUIRE, The constant property turbulent boundary layer with injection; a reanalysis of some experimental results, *Int. J. Heat Mass Transfer* **13**, 939–942 (1970).
32. R. M. KENDALL, M. W. RUBESIN, T. J. DAHM and M. R. MENDENHALL, Mass, momentum, and heat transfer within a turbulent boundary layer with foreign gas mass transfer at the surface, Part I—constant fluid properties, Report No. III, Vidya Research and Development, Palo Alto, California (February 1964).
33. D. B. SPALDING and S. W. CHI, The drag of a compressible turbulent boundary layer on a smooth flat plate with and without heat transfer, *J. Fluid Mech.* **18**, 117–143 (1964).
34. E. J. HOPKINS, M. W. RUBESIN, M. INOUYE, E. R. KEENER, G. C. MATTEER and T. E. POLEK, Summary and correlation of skin-friction and heat-transfer data for a hypersonic turbulent boundary layer in simple shapes, Compressible Turbulent Boundary Layers, a symposium held at Langley Research Center, December 1968,
35. M. H. BERTRAM, A. M. CARY, JR. and A. M. WHITEHEAD, JR., Experiments with hypersonic turbulent boundary layers on flat plates and delta wings, AGARD Specialist's Meeting on Hypersonic Boundary Layers and Flow Fields, London, England (May 1968).
36. A. V. GOMEZ, A. F. MILLS and D. M. CURRY, Correlations of heat and mass transfer for the stagnation region of a reentry vehicle with multicomponent mass addition, *Space Systems and Thermal Technology for the* 70's, Part II, ASME (June 1970).
37. A. F. MILLS and A. WORTMAN, Two-dimensional stagnation point flows of binary mixtures, *Int. J. Heat Mass Transfer* **15**, 969–987 (1972).
38. A. WORTMAN, Mass transfer in self-similar laminar boundary layer flows, Ph.D. Dissertation, School of Engineering and Applied Science, University of California, Los Angeles (1969).
39. L. LEES, Laminar heat transfer over blunt-nosed bodies at hypersonic flight speeds, *Jet Propulsion* **26**, 259–269 (1956).
40. C. C. PAPPAS and A. F. OKUNO, Measurements of skin friction of the compressible turbulent boundary layer on a cone with foreign gas injection, *J. Aero/Space Sci.* **27**, 321–333 (1960).
41. P. N. ROMANENKO and V. N. KHARCHENKO, The effect of transverse mass flow on heat transfer and friction drag in a turbulent flow of compressible gas along an arbitrarily shaped surface, *Int. J. Heat Mass Transfer* **6**, 727–738 (1963).
42. C. C. PAPPAS and A. F. OKUNO, Measurement of heat transfer and recovery factor of a compressible turbulent boundary layer on a sharp cone with foreign gas injection, NASA Technical Note D-2230 (April 1964).
43. O. E. TEWFIK. Discussion of "The effect of transverse mass flow on heat transfer and friction drag in a turbulent flow of compressible gas along an arbitrarily shaped surface," *Int. J. Heat Mass Transfer* **7**, 397–399 (1964).
44. J. E. DANBERG, Measurements of the characteristics of the compressible turbulent boundary layer with air injection, NAVORD Rep. 6683 (3 Sept. 1959).

CALCUL DE COUCHES LIMITES TURBULENTES AVEC INJECTION DE GAZ ETRANGER

Résumé—On a obtenu des solutions numériques pour des couches limites turbulentes compressibles d'air sur une plaque plane avec injection de gaz étranger en faisant l'hypothèse que l'équation de quantité de mouvement est couplée aux équations des espèces et de l'énergie seulement par les variations spatiales de la masse volumique moyenne et de la viscosité. La méthode de calcul aux différences finies comprend la transformation "ω^2" avec différence centrale. Les espèces injectées sont H_2, He, CH_4, H_2O, CO, Air, CO_2, Fréon 12, Xe et CCl_4; les rapports de température T_s/T_e varient entre 0,2 et 2 tandis que le domaine des nombres de Mach est compris entre 0 et 6. Les propriétés thermodynamiques sont estimées en tenant compte de chaleurs spécifiques variables; pour les propriétés de transport on utilise la théorie cinétique avec le potentiel de Lennard–Jones. On ignore la diffusion thermique et la conduction diffusionnelle. Des modèles de viscosité par turbulence pour la région interne ont été évaluées par comparaison avec les résultats expérimentaux relatifs aux écoulements soufflés à propriété constante, et un "meilleur" modèle a été sélectionné pour les calculs paramètriques. Les nombres de Schmidt et de Prandtl turbulents sont pris constants et valent respectivement 0,8 et 0,9. Les résultats montrent le rôle important joué par les variations de masse volumique dans la couche limité; les nombres de Stanton de transfert massique et thermique pour les injectants les plus lourds augmentent avec l'injection, et on trouve que les injectants légers sont plus efficaces dans la réduction du frottement superficiel et du transfert thermique que ne l'indiquent les résultats expérimentaux. L'accord avec l'expérience pour des écoulements à faible vitesse est généralement satisfaisant; de même l'influence du nombre de Mach sur le frottement superficiel est en relation avec l'expérience.

DIE BERECHNUNG VON TURBULENTEN GRENZSCHICHTEN MIT FREMDGAS-EINBLASUNG

Zusammenfassung—Es wurden numerische Lösungen ermittelt, für kompressible turbulente Grenzschichten in Luft, an der ebenen Platte, mit Fremdgas-Einblasung. Dabei wurde vorausgesetzt, dass die Impulsgleichung mit der Erhaltungsgleichung für die einzelnen Gaskomponenten und mit der Energiegleichung nur über die räumliche Veränderung der gesamten Dichte und Viskosität gekoppelt ist. In das Rechenverfahren mit finiten Differenzen ist die "ω^2"-Transformation mit zentralen Differenzen eingearbeitet. Die eingeblasenen Gaskomponenten umfassen H_2, He, CH_4, H_2O, Co, Luft, CO_2, Freon 12, Xe und CCl_4; die Temperaturverhältnisse T_2/T_e überstreichen den Bereich von 0,2 bis 2,0, die Mach-Zahlen den Bereich von 0 bis 6. Die thermodynamischen Eigenschaften werden so berechnet, dass variable spezifische Wärmen berücksichtigt werden können. Für die Transporteigenschaften wurde die kinetische Theorie mit dem Lennard–Jones-Potential zugrundegelegt. Thermodiffusion und Diffusionswärmeleitung sind vernachlässigt. Modelle der zusätzlichen Viskosität für die innere Zone wurden durch Vergleich mit experimentellen Daten für Strömungen mit konstanten Eigenschaften ausgewertet: daraus wurde ein "bestes" Model für die Parameter-Berechnungen ausgewählt. Die Schmidt- und Prandtl-Zahlen für Turbulenz wurden als konstant angenommen, und zwar zu 0,8 und 0,9. Die Ergebnisse zeigen den enormen Einfluss der Dichteänderung senkrecht zur Grenzschicht. Die Stanton-Zahlen für den Stoff- und Wärmeübergang steigen bei den schwersten eingeblasenen Gaskomponenten mit dem Einblasen. Bei den leichten Gaskomponenten wurde eine grössere Verringerung bei der Wandreibung und beim Wärmeübergang festgestellt als experimentelle Werte angeben. Die Übereinstimmung mit Experimenten ist für langsame Geschwindigkeiten allgemein zufriedenstellend; ebenso ist der berechnete Einfluss der Mach-Zahl auf die Wandreibung in Übereinstimmung mit Experimenten.

РАСЧЕТ ТУРБУЛЕНТНЫХ ПОГРАНИЧНЫХ СЛОЕВ С ВДУВОМ ИНОРОДНОГО ГАЗА

Аннотация—Получены численные решения для сжимаемых турбулентных пограничных слоев воздуха с вдувом инородного газа на плоской пластине на основании гипотезы о том, что уравнение количества движения связано с уравнением энергии только через пространственные изменения плотности и вязкости. Методика расчета в конечных разностях включает преобразование «ω^2» с помощью центральных разностей. Вдувались воздух, H_2, He, CH_4, H_2O, CO, CO_2, фреон -12, Xe и CCl_4. Температурные отношения T_s/T_e колебались от 0,2 до 2,0, тогда как значения числа Маха изменялись

от 0 до 6. Учитывалось изменение удельных теплоемкостей; для учета свойств переноса использовалась кинетическая теория с потенциалом Леннарда-Джонса. Тепловая диффузия и диффузионный перенос во внимание не принимались. Модели турбулентной вязкости для внутренней области оценивались путем сравнения с экспериментальными данными для потоков жидкости с постоянными свойствами и «наилучшей» моделью, выбранной для параметрических расчетов. Турбулентные числа Шмидта и Прандтля принимались постоянными, равными соответственно 0,8 и 0,9. Результаты свидетельствуют о важной роли изменения плотности поперек пограничного слоя. Тепло-и массообменные числа Стантона при вдуве наиболее тяжелых газов заметно увеличиваются, а легкие газы способствуют уменьшению поверхностного трения и теплообмена сильнее, чем о том говорят экспериментальные данные. Показано, что соответствие с экспериментальными данными для малоскоростных потоков, в общем, удовлетворительно, а расчетное влияние числа Маха на поверхностное трение также согласуется с экспериментом.